



Tetraspanin-13 modulates voltage-gated $\text{Ca}_v2.2$ Ca^{2+} channels

SUBJECT AREAS:

CELLULAR
NEUROSCIENCE

PROTEIN-PROTEIN INTERACTION
NETWORKS

CALCIUM CHANNELS

ION CHANNELS IN THE
NERVOUS SYSTEM

Robert T. Mallmann^{1,2*}, Thomas Wilmes^{1*}, Lucia Lichvarova³, Anja Bühner^{1,2}, Barbara Lohmüller^{1,2}, Jan Castonguay¹, Lubica Lacinova³ & Norbert Klugbauer¹

¹Institut für Experimentelle und Klinische Pharmakologie und Toxikologie, Albert-Ludwigs-Universität Freiburg, 79104 Freiburg, Germany, ²Fakultät für Biologie, Albert-Ludwigs-Universität Freiburg, 79104 Freiburg, Germany, ³Institute for Molecular Physiology and Genetics, 83334 Bratislava, Slovakia.

Integration of voltage-gated Ca^{2+} channels in a network of protein-interactions is a crucial requirement for proper regulation of channel activity. In this study, we took advantage of the specific properties of the yeast split-ubiquitin system to search for and characterize so far unknown interaction partners of Ca_v2 Ca^{2+} channels. We identified tetraspanin-13 (TSPAN-13) as an interaction partner of the α_1 subunit of N-type $\text{Ca}_v2.2$, but not of P/Q-type $\text{Ca}_v2.1$ or L- and T-type Ca^{2+} channels. Interaction could be located between domain IV of $\text{Ca}_v2.2$ and transmembrane segments S1 and S2 of TSPAN-13. Electrophysiological analysis revealed that TSPAN-13 specifically modulates the efficiency of coupling between voltage sensor activation and pore opening of the channel and accelerates the voltage-dependent activation and inactivation of the Ba^{2+} current through $\text{Ca}_v2.2$. These data indicate that TSPAN-13 might regulate $\text{Ca}_v2.2$ Ca^{2+} channel activity in defined synaptic membrane compartments and thereby influences transmitter release.

Received
12 December 2012

Accepted
18 April 2013

Published
7 May 2013

Correspondence and requests for materials should be addressed to N.K. (n.klugbauer@pharmakol.uni-freiburg.de)

* These authors contributed equally to this work.

In the nervous system, presynaptic Ca^{2+} channels of the Ca_v2 family including $\text{Ca}_v2.1$ and $\text{Ca}_v2.2$ play pivotal roles in the Ca^{2+} -dependent neurotransmitter release¹. Their activity is tightly regulated by a multitude of adjacent proteins forming defined interaction platforms. Innovative and comprehensive experimental approaches like the use of affinity purification and quantitative mass spectrometry have systematically characterized Ca_v2 Ca^{2+} channel nanodomains^{2,3}. Even though these and other studies shed light on the complex protein networks involved in the subtype-specific modulation of Ca_v2 family members, many aspects underlying their regulation remain unknown and could probably be accredited to yet unidentified interaction partners. Different methodical approaches aiming at the identification of Ca^{2+} channel interaction partners might favour certain protein-protein interactions based on their biochemical character. Therefore the use of alternative methods to characterize the interactome of Ca^{2+} channels is desirable.

Screening of cDNA libraries using specific bait proteins in yeast two-hybrid (YTH) assays has revealed so far unknown protein-protein interactions, which often are essential for complex regulatory mechanisms⁴. The use of $\text{Ca}_v2.1$ and $\text{Ca}_v2.2$ domains as bait proteins in a classical YTH system identified active zone RIM proteins as being presynaptic Ca^{2+} channel tethering adapter molecules that facilitate fast and synchronous neurotransmitter release⁵. However, due to intrinsic limitations of the classical YTH system, interactions between hydrophobic membrane proteins are not detected. A modified YTH system makes use of a split-ubiquitin which reconstitutes upon interaction of fused bait and prey proteins allowing for the detection of protein-protein interactions within or close to plasma membranes⁶. This experimental setup enables the identification and characterization of so far unknown interaction partners of Ca_v2 family members, which might comprise membrane proteins important for modulation of individual Ca_v2 functions.

Results

$\text{Ca}_v2.2$ α_1 subunit interacts with tetraspanin-13. In order to identify and characterize novel interaction partners of presynaptic Ca^{2+} channels, we constructed bait vectors encoding $\text{Ca}_v2.1$ and $\text{Ca}_v2.2$ Ca^{2+} channel α_1 subunit cDNA-fragments. Since our attempts to express full-length α_1 subunit cDNA in yeast cells failed, we constructed bait-vectors encoding single domains and C-terminal fragments. We hypothesized that putative novel interaction partners might bind to the rather long intracellular C-terminus of Ca_v2 channels and selected domain IV as a kind of “membrane anchor” fused to the C-terminus. This construct also takes into account that putative interaction partners might bind not only to the C-terminus, but also to parts of the smaller intracellular loops within domain IV or even its transmembrane segments.



Amongst several candidate proteins TSPAN-13, a member of the tetraspanin family of membrane proteins demonstrated robust interaction with domain IV of the $\text{Ca}_v2.2 \alpha_1$ subunit. The usage of a series of truncated forms identified the entire domain IV of the $\text{Ca}_v2.2 \alpha_1$ subunit to be critical for the interaction with TSPAN-13 (Fig. S1a online). Interaction was confirmed by co-immunoprecipitation of $\text{Ca}_v2.2$ -EGFP with TSPAN-13-Myc expressed in CHO cells (Fig. 1).

Tetraspanins, as implicated by its names, consist of four transmembrane segments and are characterized by a long extracellular loop (LEL) containing a conserved CCG motif⁷. Using a yeast pellet- β -galactosidase assay⁷ we analysed the interaction between different TSPAN-13 deletion mutants with domain IV of the $\text{Ca}_v2.2 \alpha_1$ subunit. Remarkably, the interaction between TSPAN-13 and $\text{Ca}_v2.2$ was not affected by deletion of transmembrane segment S3 and S4, the LEL and the C-terminus of TSPAN-13 in the mutant TSPAN-13 $_{\Delta(S3-Ct)}$ (Fig. S1b online). Interaction between TSPAN-13 $_{\Delta(S3-Ct)}$ and domain IV of $\text{Ca}_v2.2$ was confirmed by a yeast β -galactosidase filter-lift assay. Expression of TSPAN-13 in the murine brain was demonstrated by an RT-PCR analysis (Fig. S2 online). We identified TSPAN-13 mRNA at about equal levels in the hippocampus, neocortex and cerebellum.

TSPAN-13 affects Ca^{2+} -currents in NG108-15 cells. Since Ca_v channel activity depends on the integrity of complex protein networks, which contain a multitude of Ca_v channel interaction partners, we analysed whether TSPAN-13 affects channel properties of its putative interaction partner $\text{Ca}_v2.2$ using differentiated NG108-15 cells. Upon cultivation in the presence of cAMP, these cells express representatives of high-voltage-activated L-type and non-L-type (predominantly N-type) and low-voltage-activated T-type Ca^{2+} channels⁸⁻¹⁰. We compared whole-cell currents measured from differentiated NG108-15 cells transfected either with a control EGFP-vector or with a vector encoding TSPAN-13-EGFP. Amplitudes of low-voltage-activated Ca^{2+} currents activated by depolarization up to -20 mV were not affected by TSPAN-13 (Fig. 2a and b). In contrast, high-voltage-activated Ba^{2+} current amplitude activated by depolarization to 0 mV and above was significantly decreased (unpaired two-tail t-test; 0 mV: $p = 0.0167$; +10 mV: $p = 0.0270$; +20 mV: $p = 0.0177$; +30 mV: $p = 0.0177$). High-voltage activated Ca^{2+} channels were pharmacologically classified. P/Q type ($\text{Ca}_v2.1$) channels are absent in NG108-15 cells, since in agreement with observations by Liu and colleagues⁹, we have seen no effect of 500 nM ω -agatoxin on whole-cell Ba^{2+} current. The specific N-type channel blocker ω -conotoxin GVIA blocked $33 \pm 12\%$ (mean \pm SD; $n = 10$) of total current amplitude. The remaining current can be ascribed to L-type Ca^{2+} channels. As the variability of the proportion of channel subtypes in individual cells was high, we turned to recombinant systems.

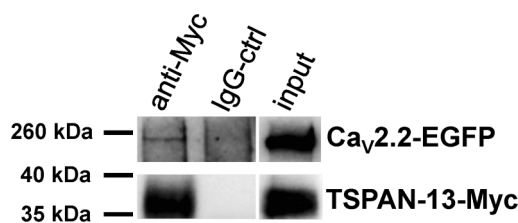


Figure 1 | Co-immunoprecipitation analysis using solubilisates of membrane-fractions obtained from CHO cells expressing $\text{Ca}_v2.2$ -EGFP and transiently transfected with TSPAN-13-Myc. Eluates from co-immunoprecipitations with either anti-Myc (left) or IgG-control antibodies (middle) and the input controls (right) were separated on 7% ($\text{Ca}_v2.2$ -EGFP) or 12% (TSPAN-13-Myc) SDS-polyacrylamide gels, respectively. Shown is a representative example of three independent co-immunoprecipitation experiments. The figure shows the relevant area of the antibody-staining.

Effects of TSPAN-13 on recombinant $\text{Ca}_v1.2$, $\text{Ca}_v2.2$ and $\text{Ca}_v3.1 \text{Ca}^{2+}$ -channels. Next, we confirmed these results using cell lines expressing recombinant $\text{Ca}_v \text{Ca}^{2+}$ channels co-transfected either with a control EGFP-vector or with a vector encoding TSPAN-13-EGFP. TSPAN-13 did not affect recombinant $\text{Ca}_v1.2$ and $\text{Ca}_v3.1 \text{Ca}^{2+}$ current (Fig. 2c and d) and also did not significantly suppress current amplitude through recombinant $\text{Ca}_v2.2$ (Fig. 2e). Neither in NG108-15 nor in CHO cells the inhibition of the N-type Ca^{2+} current was accompanied by a shift of the I-V relationship. In contrast to CHO cells, NG108-15 cells do express a considerable outwards K^{+} current. This current was probably responsible for an apparent shift of the reversal potential which was observed in NG108-15 cells (Fig. 2b), but was much less pronounced in CHO cells (Figure 2e).

This result points out that TSPAN-13 might have a specific functional impact on $\text{Ca}_v2.2 \text{Ca}^{2+}$ channels. TSPAN-13 suppressed the amplitude of current through $\text{Ca}_v2.2$ channels in NG108-15 cells and also in a cell line expressing $\text{Ca}_v2.2$ (Fig. 2e), though, the latter was statistically not significant. We optimized the voltage protocols for the analysis of possible effects of TSPAN-13 on current kinetics (Fig. 3). TSPAN-13 significantly accelerated the kinetics of Ba^{2+} current activation (Fig. 3a) when time constants at individual depolarisations were compared. This acceleration was due to a shift of the voltage dependence of the activation time constant towards less depolarized membrane potentials (Table S1 online). Further, TSPAN-13 significantly accelerated the inactivation of Ba^{2+} current due to an enhanced proportion of the current inactivating with a fast time constant (Fig. 3b and Table 1). To visualise this effect we constructed model time courses of fast and slow components of both currents (Fig. 3b). To analyse if TSPAN-13 may affect the Ca^{2+} -dependent inactivation of the $\text{Ca}_v2.2$ channel we repeated these experiments using Ca^{2+} as a charge carrier (Fig. 3c and d). Ca^{2+} current through the $\text{Ca}_v2.2$ channel activated about twice as fast as the Ba^{2+} current (Fig. 3c versus 3a). Co-expression of TSPAN-13 enhanced the activation time constants at individual depolarisations (Fig. 3c), but this effect was not significant. Nevertheless, TSPAN-13 significantly decreased the steepness of the voltage dependence of Ca^{2+} current activation (Table S1 online). Inactivation of Ca^{2+} current through the $\text{Ca}_v2.2$ channel was not significantly altered by TSPAN-13 (Fig. 3d).

An accelerated voltage-dependent inactivation suggests that TSPAN-13 may affect the cumulative inactivation during action potential bursts. Indeed, the total inactivation at the end of a series of action-potential-like waveforms or at the end of a high-frequency series of short depolarising pulses was enhanced by TSPAN-13, nevertheless, this effect was not significant (Fig. S3a, b, c online). Similarly, the facilitation of recovery from voltage-dependent inactivation by TSPAN-13 was not statistically significant (Fig. S3d and Table S2 online).

Further, we sought for effects of TSPAN-13 on gating currents, which reflect the activation process of the voltage sensor.

TSPAN-13 affects gating currents of $\text{Ca}_v2.2$ channels. We measured gating currents of $\text{Ca}_v2.2$ channels by depolarizing each cell to its reversal potential (Fig. 4a). The maximal charge Q_{max} evaluates as an area below the gating current trace and is indicative for the number of channels expressed in the cell membrane. This value was not affected by co-expression of TSPAN-13. In addition, the kinetics of the charge movement was not changed. The time constants of the decay of the gating current traces were 0.54 ± 0.02 ms ($n = 12$) and 0.58 ± 0.02 ms ($n = 12$) for control and TSPAN-13-transfected cells, respectively.

Next, we compared the relationship between the maximal conductance G_{max} and the maximal charge Q_{max} for each cell (Fig. 4b). This term reflects the efficiency of the coupling between the voltage sensor activation and the pore opening¹¹. We found that the $G_{\text{max}}/Q_{\text{max}}$

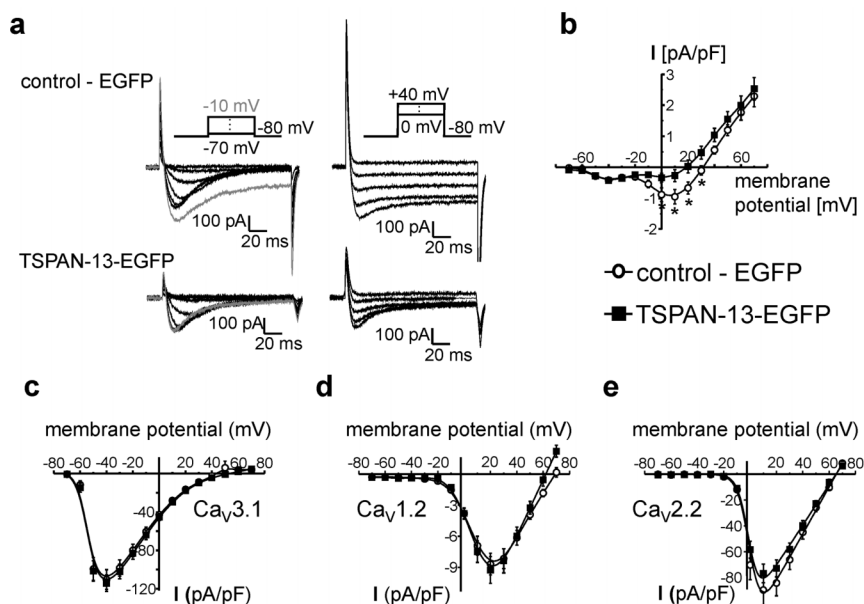


Figure 2 | Functional characterization of the interaction of TSPAN-13 with different classes of voltage gated Ca^{2+} channels. (a) Representative examples of current traces recorded from differentiated NG108-15 cells transfected either with an EGFP control plasmid or with a plasmid encoding TSPAN-13-EGFP. Current traces activated by depolarizing pulses with amplitudes between -70 mV and -10 mV and between 0 mV and $+40$ mV are presented separately. (b) Averaged current-voltage (I-V) relationships constructed from peak current amplitudes measured as illustrated in panel A. \circ - cells transfected with an EGFP control plasmid ($n = 26$); \blacksquare - cells transfected with a plasmid encoding TSPAN-13-EGFP ($n = 26$). (c) I-V relationship for the recombinant $\text{Ca}_v3.1$ channel stably expressed in a HEK 293 cell line. \circ - cells co-transfected with an EGFP control plasmid ($n = 22$); \blacksquare - cells co-transfected with a plasmid encoding TSPAN-13-EGFP ($n = 19$). (d) I-V relationship for the recombinant $\text{Ca}_v1.2$ channel stably expressed in a HEK 293 cell. \circ - cells co-transfected with an EGFP control plasmid ($n = 18$); \blacksquare - cells co-transfected with a plasmid encoding TSPAN-13-EGFP ($n = 20$). (e) I-V relationship for the recombinant $\text{Ca}_v2.2$ channel stably expressed in a CHO cell line. \circ - cells co-transfected with an EGFP control plasmid ($n = 16$); \blacksquare - cells co-transfected with a plasmid encoding TSPAN-13-EGFP ($n = 15$).

relationship is less steep in the presence of TSPAN-13. The averaged G_{\max}/Q_{\max} values were 0.19 ± 0.01 nS/fC ($n = 13$) and 0.15 ± 0.01 nS/fC ($n = 12$) for control and TSPAN-13-transfected cells, respectively (Fig. 3c). These values were significantly different (unpaired two-tail t-test $p = 0.0026$). The effect of TSPAN-13 on channel gating is in agreement with the observed shift of the voltage dependence of $\tau_{\text{act}}(V)$ along the voltage axes (V_{tact}) (Table S1 online).

As for full-length TSPAN-13, we used the G_{\max}/Q_{\max} relationship as an indicator for a functional modulation of $\text{Ca}_v2.2$ by various TSPAN-13 constructs (Fig. 4c). Since the deleted segments S3 and S4 could be crucial for the functional modulation of $\text{Ca}_v2.2$ by TSPAN-13, we analysed whether the G_{\max}/Q_{\max} relationship is still affected by expression of TSPAN-13 $_{\Delta(S3-C)}$. In the presence of TSPAN-13 $_{\Delta(S3-C)}$, G_{\max}/Q_{\max} was significantly decreased from 0.18 ± 0.01 nS/fC to 0.14 ± 0.01 nS/fC (unpaired two-tail t-test $p = 0.0049$) (Fig. 4c). These data indicate that the modulation of $\text{Ca}_v2.2$ by TSPAN-13 is preserved in the absence of S3 and S4, the LEL and the C-terminus.

Point mutations within TSPAN-13 identify critical amino acid residues for channel modulation. The transmembrane segments S1 and S2 of tetraspanins contain highly conserved amino acid residues which have been shown to mediate tight interactions between both transmembrane domains^{12,13}. The TSPAN-13 transmembrane segments S1 and S2 include several bulky amino acid residues which might be involved in these interactions. Thus, we mutated these candidate amino acids and analysed whether the G_{\max}/Q_{\max} relationship is affected by expression of TSPAN-13 constructs containing single amino acid mutations in $\text{Ca}_v2.2$ -expressing cells.

The mutation of two phenylalanine residues located at positions 55 and 57 in segment S2 to alanine abolished the reduction of

G_{\max}/Q_{\max} which was observed in the presence of TSPAN-13. In control cells, G_{\max}/Q_{\max} was 0.18 ± 0.01 nS/fC while in the presence of TSPAN-13 $_{(F55A)(F57A)}$ G_{\max}/Q_{\max} was 0.17 ± 0.01 nS/fC (no significant difference) (Fig. 4c). We further analysed whether a single mutation of F55A or F57A is sufficient to abolish the modulation of the G_{\max}/Q_{\max} relationship. Indeed, the expression of TSPAN-13 $_{(F55A)}$ or TSPAN-13 $_{(F57A)}$ did not significantly affect G_{\max}/Q_{\max} compared with controls (0.19 ± 0.01 nS/fC to 0.20 ± 0.01 nS/fC or 0.19 ± 0.01 nS/fC to 0.20 ± 0.01 nS/fC, respectively). We further estimated the protein expression level of several TSPAN-13 constructs to ensure that the missing modulatory effect of the TSPAN-13 point mutations is not simply caused by a reduced expression level. Four independent transfection experiments and Western blot analyses were performed using EGFP-tagged TSPAN-13 constructs (Fig. S4 online). Compared to TSPAN-13 the mutant constructs displayed expression levels that are not significantly different to each other. In fact we even observed a slightly higher expression of the TSPAN-13 $_{(F55A)(F57A)}$ mutant.

In summary, these data indicate that amino acid residues F55 and F57 located within S2 are essential for the modulation of $\text{Ca}_v2.2$ currents by TSPAN-13. To rule out an influence of these mutations on the intracellular localization of TSPAN-13, which might suppress its membrane trafficking and thereby indirectly prevent an interaction between TSPAN-13 and $\text{Ca}_v2.2$, we analysed the intracellular localization of TSPAN-13 mutants F55A, F57A and F55A&F57A. All mutants co-localized with the membrane marker Akt-PH-mCherry and showed a distribution similar to TSPAN-13 making perturbations of intracellular protein localization an unlikely explanation for the observed abrogation of $\text{Ca}_v2.2$ modulation (Fig. 5). We further mutated a tryptophan residue located within S1 (W33A) to analyse for a possible role in $\text{Ca}_v2.2$ modulation by TSPAN-13. However, expression of TSPAN-13 $_{(W33A)}$ caused a significant reduction of

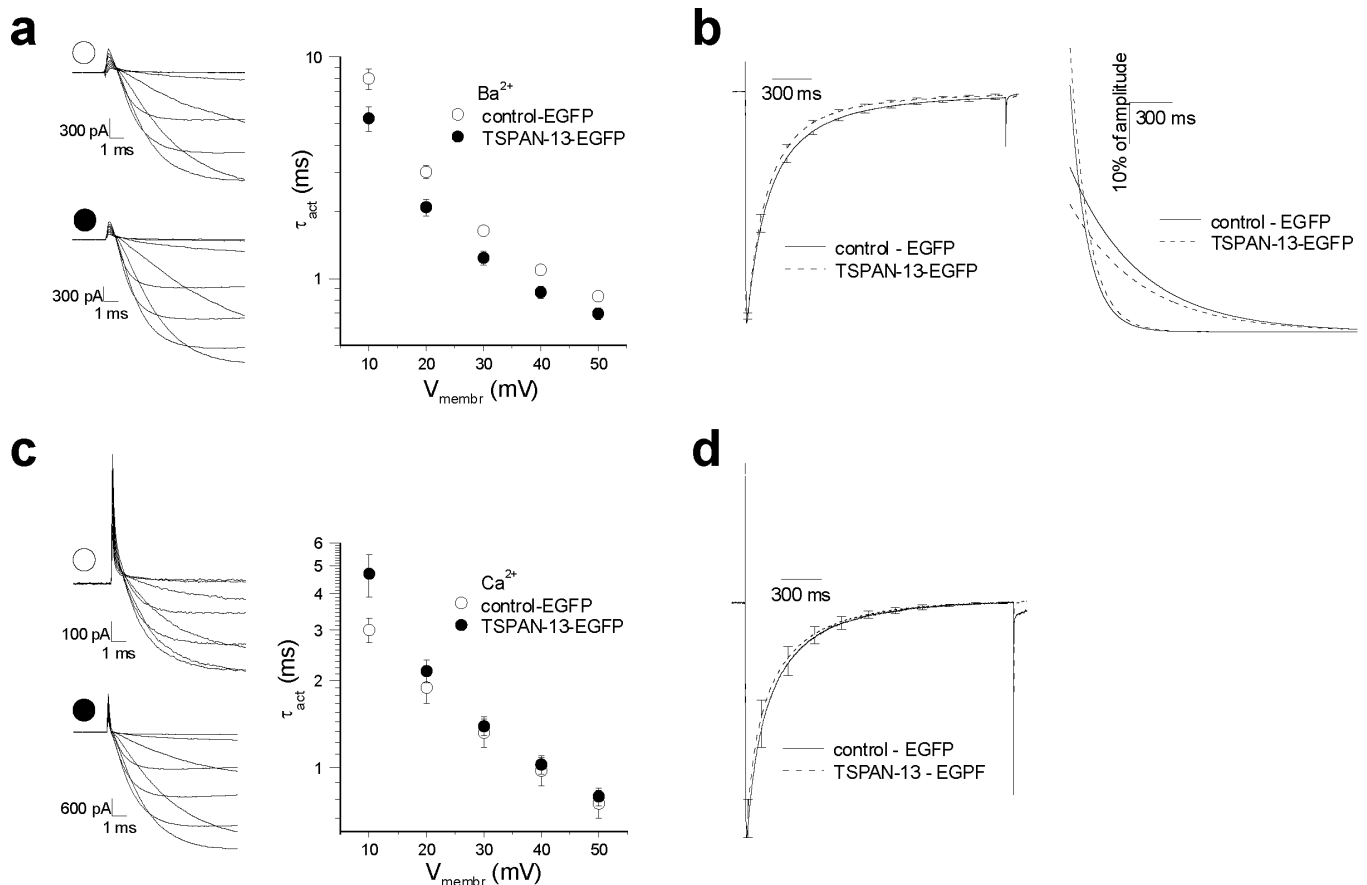


Figure 3 | Activation and inactivation kinetics of the current through Ca_v2.2 channels stably expressed in CHO cells. (a) Examples of current traces recorded by 10 ms long depolarisations from a holding potential of -80 mV to potentials increasing from -10 mV up to $+50$ mV with a step of 10 mV. Ba²⁺ was used as charge carrier. Cells were either transfected with an EGFP control plasmid ($n = 18$) or with a plasmid encoding TSPAN-13-EGFP ($n = 19$). Current traces activated by depolarisations to $+10$ mV and higher were fitted by a single exponential and corresponding time constants were averaged and plotted in the graph. The significance of the difference between time constants determined for individual depolarisations was tested by the unpaired two-tail t-test ($+10$ mV, $p = 0.018$; $+20$ mV, $p = 0.0017$; $+30$ mV, $p = 0.0016$; $+40$ mV, $p = 0.0027$; $+50$ mV, $p = 0.0100$). (b) Averaged current traces recorded by 2 s long depolarizations from a holding potential of -80 mV to $+20$ mV (peak of an IV). Ba²⁺ was used as charge carrier. Cells were either transfected with an EGFP control plasmid (solid line; $n = 22$) or with a plasmid encoding TSPAN-13-EGFP (dashed line; $n = 20$). Each trace was fitted by a sum of two exponentials. The right part of the panel shows both, the fast and slow components which were simulated using the averaged time constants and relative amplitudes listed in table 1. (c) Examples of current traces recorded using the same protocol as in (a). Ca²⁺ was used as charge carrier. Cells were either transfected with an EGFP control plasmid ($n = 11$) or with a plasmid encoding TSPAN-13-EGFP ($n = 14$). Current traces activated by depolarisations to $+10$ mV and higher were fitted by a single exponential and corresponding time constants were averaged and plotted in the graph. (d) Averaged current traces recorded by 2 s long depolarisations from a holding potential of -80 mV to $+20$ mV (peak of an IV). Ca²⁺ was used as charge carrier. Cells were either transfected with an EGFP control plasmid (solid line; $n = 8$) or with a plasmid encoding TSPAN-13-EGFP (dashed line; $n = 12$).

G_{\max}/Q_{\max} compared with controls (0.20 ± 0.01 nS/fC to 0.17 ± 0.01 nS/fC, (unpaired two-tail t-test $p = 0.0020$)). This reduction was similar to the effect of TSPAN-13 and makes an involvement of W33 in Ca_v2.2 modulation unlikely.

The N-terminus is important for membrane localization of TSPAN-13. Next, we analysed the importance of the N-terminus of TSPAN-13 for the modulation of Ca_v2.2, by constructing a deletion mutant of TSPAN-13 lacking the intracellular N-terminus. By co-transfection of TSPAN-13_{ΔNt} the TSPAN-13 mediated reduction of G_{\max}/Q_{\max} in Ca_v2.2 expressing cells was abolished. While G_{\max}/Q_{\max} was 0.20 ± 0.01 nS/fC in the presence of TSPAN-13_{ΔNt} corresponding controls showed similar values (0.21 ± 0.01 nS/fC; not significant). Importantly, the TSPAN-13_{ΔNt} mutant did not co-localize with the membrane marker Akt-PH-mCherry (Fig. 5). TSPAN-13_{ΔNt} was rather found in intracellular compartments that potentially resemble the endoplasmic reticulum. We assume that the N-terminus of TSPAN-13 is

required for its correct intracellular targeting and that modulation of Ca_v2.2 is abolished because of the absence of TSPAN-13_{ΔNt} from the plasma membrane.

Tetraspanin CD81 does not modulate Ca_v2.2. In order to demonstrate that modulation of Ca_v2.2 is not a general property of all members of the tetraspanin family, we investigated the functional role of tetraspanin CD81. In another screening experiment using the split-ubiquitin system we searched for interaction partners of the L-type Ca²⁺ channel Ca_v1.2 α_1 subunit. Again we used single domains as bait constructs and identified CD81 as a potential interaction partner of the Ca_v1.2 α_1 subunit. A potential modulatory effect of CD81 on Ca_v2.2 was investigated by electrophysiological analysis. The corresponding G_{\max}/Q_{\max} values were 0.22 ± 0.01 ($n = 11$) and 0.19 ± 0.01 ($n = 9$) for control cells and CD81-transfected cells, respectively. These values were not significantly different, indicating that modulation of Ca_v2.2 is specific for TSPAN-13.



Table 1 | Effect of TSPAN-13 on the inactivation kinetics of Ba^{2+} and Ca^{2+} currents through $Ca_v2.2$. Individual current traces demonstrated in figure 3b and 3d were fitted by a sum of two exponentials. Resulting time constants τ_{fast} and τ_{slow} as well as the relative amplitude A1 of the current inactivating with the fast time constant τ_{fast} are summarized in the table. The relative amplitude A2 of the current inactivating with the fast time constant τ_{slow} is 100% - A1. Significance of differences between control cells and cells expressing TSPAN-13 were tested by unpaired two-tail t-test. *, $p = 0.0255$

	A1 (%)	τ_{fast} (ms)	τ_{slow} (ms)	n
Ba^{2+} control-EGFP	$60 \pm 3^*$	122 ± 6	483 ± 22	22
Ba^{2+} TSPAN-13-EGFP	$69 \pm 2^*$	126 ± 2	494 ± 29	20
Ca^{2+} control-EGFP	54 ± 4	93 ± 18	358 ± 37	8
Ca^{2+} TSPAN-13-EGFP	55 ± 5	106 ± 17	367 ± 46	12

Discussion

In this study we took advantage of the specific qualities of the yeast split-ubiquitin system to further define the interactome of voltage-gated Ca^{2+} channels and have characterized TSPAN-13 as an interaction partner of the $Ca_v2.2$ Ca^{2+} channel α_1 subunit. The tetraspanin family of membrane proteins is defined by its consensus structure comprising four transmembrane segments, two characteristic extracellular loops and a conserved CCG motif⁴. The small and large extracellular loops are located between transmembrane segments S1&2 and S3&4, respectively^{15–17}. The large extracellular loop has been described to be essential for the function of different

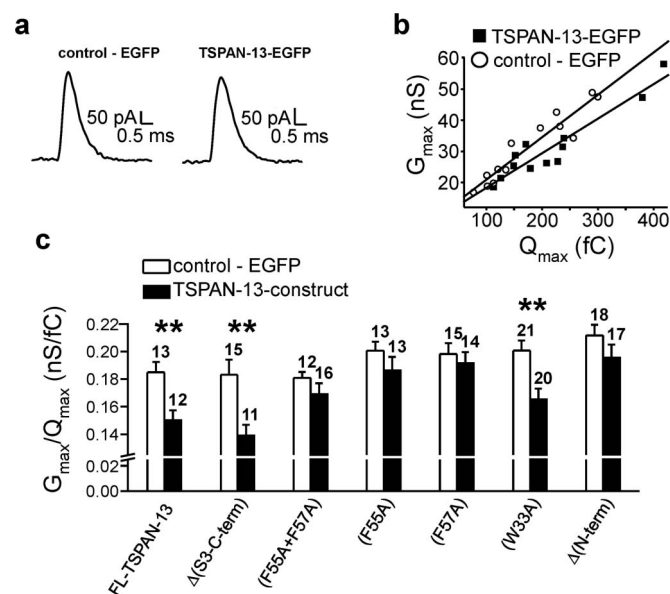


Figure 4 | Effect of TSPAN-13 on gating currents of $Ca_v2.2$ channels expressed in CHO cells and determination of the G_{max}/Q_{max} ratio. (a) Examples of current traces recorded by depolarization from a holding potential of -80 mV to the potential corresponding to the reversal potential of the investigated cell. Data represent the average of five runs. Cells were either transfected with an EGFP control plasmid or with a plasmid encoding TSPAN-13-EGFP. (b) G_{max} versus Q_{max} for control cells (\circ) and cells transfected with TSPAN-13 (\blacksquare). Straight lines represent linear fits of experimental data. (c) G_{max}/Q_{max} ratio for TSPAN-13 and various TSPAN-13 constructs. Number of cells tested is indicated at each column. ** - significantly different from control, $p < 0.01$. Abbreviations: FL-TSPAN-13, full-length-TSPAN-13; δ , regions that are deleted in TSPAN-13 constructs.

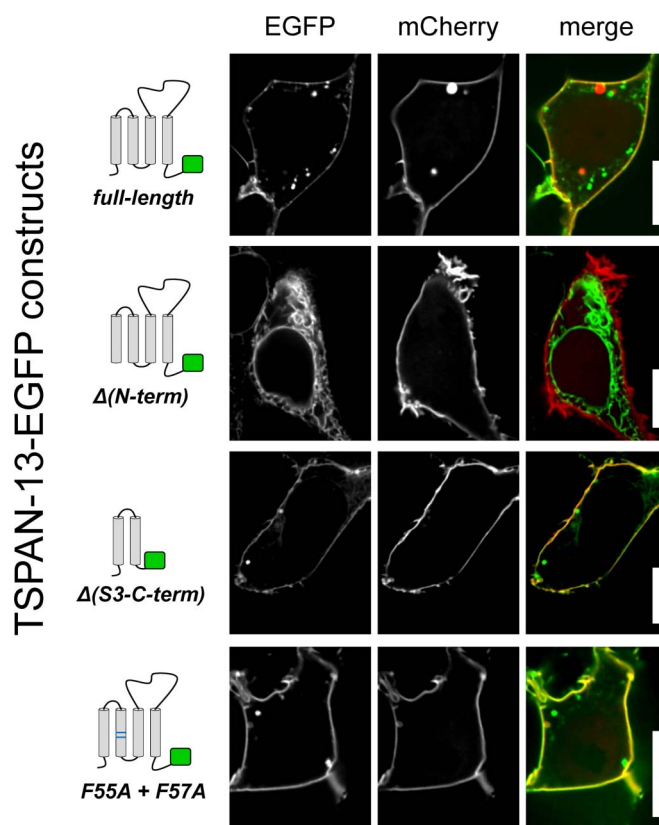


Figure 5 | Intracellular localisation of full-length TSPAN-13-EGFP and mutant forms of TSPAN-13-EGFP expressed in HEK293 cells using pAkt-PH-mCherry as membrane marker. In contrast to full-length TSPAN-13, the $\Delta(S3-C-term)$ mutant and TSPAN-13(F55A,F57A) mutant, the N-terminal TSPAN-13 deletion mutant does not localise to the plasma membrane. First column: TSPAN-13-EGFP constructs used in this study; second column: EGFP fluorescence of TSPAN-13 constructs; third column: red fluorescence of pAkt-PH-mCherry membrane marker; fourth column: merged images. Confocal images were recorded 48 h after transfection.

tetraspanins by facilitation of protein-protein interactions^{18–20}. A multitude of interactions between ubiquitously expressed tetraspanins themselves and other membrane proteins typically leads to the formation of the so-called tetraspanin web. Tetraspanin-enriched microdomains are involved in a variety of cellular processes as diverse as cell migration, intracellular trafficking, cell fusion and signalling^{16,21,22}. However, an interaction of tetraspanins with voltage-gated Ca^{2+} channels has not been described so far.

In order to demonstrate a broad expression of TSPAN-13 in the brain, we performed an RT-PCR analysis. TSPAN-13 encoding mRNA was found in the hippocampus, neocortex and cerebellum. Currently an investigation of TSPAN-13 expression at the protein level was not accomplishable since tetraspanins are extremely homologous to each other, thereby limiting the availability of specific antibodies. Furthermore, many tetraspanins are not sufficiently immunogenic to yield reliable antibodies. Hence, a detailed characterization of tetraspanin-associated proteins and functions is difficult to accomplish and studies are currently restricted to a few tetraspanin members²².

We found that the modulatory effects of TSPAN-13 are specific for N-type channels and do not occur with L- and T-type Ca^{2+} channels. This interaction was not identified by a recently published quantitative proteomic approach of Ca_v2 channels³. We assume that different methodical approaches favour the identification of certain protein-protein interactions based on their biochemical character. A



hydrophobic interaction between transmembrane segments may be lost due to stringent solubilisation and/or co-immunoprecipitation conditions. In fact, it is the strength of our study, to identify interaction partners which could not be detected by other methods. For sure each method has its advantages and disadvantages and probably only their combination gives a more complete map of the $\text{Ca}_v2.2$ interactome.

The interaction between TSPAN-13 and $\text{Ca}_v2.2$ could be located to the membrane-spanning domain IV of the $\text{Ca}_v2.2 \alpha_1$ subunit. The regions of TSPAN-13 required for interaction and modulation of $\text{Ca}_v2.2$ could be narrowed down to a truncated version of TSPAN-13 encompassing the N-terminus and transmembrane segments S1 and S2. Sequence analysis of TSPAN-13 segments S1 and S2 indicates the presence of highly conserved amino acids which have been shown to mediate tight interactions between both transmembrane domains^{12,13}. Mutations of these key residues perturbed intramolecular tetraspanin interactions causing protein destabilization¹².

Importantly, we identified single hydrophobic amino acids located within transmembrane segment S2 to be crucial for the interaction between TSPAN-13 and $\text{Ca}_v2.2$. Because of the hydrophobic nature of domain IV of $\text{Ca}_v2.2$ and S2 of TSPAN-13, we assume that the interaction between both proteins is hydrophobic and takes place inside the membrane environment.

While membrane localization of full-length TSPAN-13 was in agreement with previous studies, where a TSPAN-13-EGFP fusion protein also localized to the plasma membrane in breast cancer cells²³, TSPAN-13_{ΔNt} was rather found in intracellular compartments, presumably the endoplasmic reticulum. Therefore, we assume that the N-terminus of TSPAN-13 is required for its correct intracellular targeting and that the lack of $\text{Ca}_v2.2$ modulation is caused by the absence of TSPAN-13_{ΔNt} from the plasma membrane.

The specific interaction between TSPAN-13 and $\text{Ca}_v2.2$, which we observed in the yeast two hybrid system and by co-immunoprecipitation has also specific functional consequences. Our electrophysiological analysis revealed that TSPAN-13 suppressed the amplitude of current through $\text{Ca}_v2.2$ channels in NG108-15 cells. It modulated the voltage-dependent activation and inactivation kinetics of $\text{Ca}_v2.2$ expressed in the CHO cells in a complex way. Reduction of the $G_{\text{max}}/Q_{\text{max}}$ ratio by an unaltered Q_{max} suggests a lowered opening probability, which is consistent with the observed decrease in the current amplitude. An altered voltage-dependence of $\tau_{\text{act}}(V)$ is consistent with modulation of channel gating^{24,25}. TSPAN-13 facilitated the voltage-dependent channel gating when Ba^{2+} was used as a charge carrier. Ca^{2+} -dependent inactivation of the $\text{Ca}_v2.2$ channel remains controversial. While it is generally accepted that calmodulin interacts with $\text{Ca}_v2.2$ channels^{26,27}, its effects on current kinetics were reported by some authors^{26,28}, but questioned by others²⁹. In our settings Ba^{2+} and Ca^{2+} currents inactivated with similar kinetics. TSPAN-13 did not alter the inactivation kinetics of the Ca^{2+} current suggesting that it probably does not interfere with the IQ motif.

The Ca^{2+} current activated faster than the Ba^{2+} current and was modulated differently by TSPAN-13. The lowered slope factor of the voltage-dependence of $\tau_{\text{act}}(V)$ is consistent with a lowered sensitivity of the channels voltage sensor^{24,25}.

Activation kinetics of $\text{Ca}_v2.2$ channels is modulated by G-proteins which constitutively inactivate the channel and this inactivation is relieved by a strong depolarisation called prepulse facilitation^{30,31}. However, prepulse facilitation was not altered by TSPAN-13 (Fig. S5 online), therefore we can exclude an interaction between TSPAN-13 and G-proteins.

We assume that the physiologic effect of TSPAN-13 on $\text{Ca}_v2.2$ channels may be much more pronounced as indicated by our characterization based on a recombinant system. In fact in NG108-15 cells we observe a significant suppression of the current through $\text{Ca}_v2.2$ channels, this suppression is not significant in CHO cells expressing $\text{Ca}_v2.2$ and TSPAN-13. In our view these results indicate

that the pure recombinant system lacks further important interaction partners which are present in NG108-15 cells. Therefore our recombinant electrophysiological experiments may only partially describe the actual effect of TSPAN-13 on $\text{Ca}_v2.2$ channels.

Another member of the tetraspanins, CD81 was not able to modulate $\text{Ca}_v2.2$ channels. We assume that the modulation by TSPAN-13 represents a novel mechanism for regulation of $\text{Ca}_v2.2 \text{Ca}^{2+}$ channel activity, thereby affecting presynaptic transmitter release. The presence of TSPAN-13 in defined synaptic membrane compartments could exclusively influence $\text{Ca}_v2.2$ mediated transmitter release.

Methods

Split-ubiquitin yeast two-hybrid screening. The Split-ubiquitin system (DUALmembrane kit 3) together with a mouse brain cDNA library (pNubGx) were purchased from Dualsystems Biotech (Zurich, Switzerland). Construction of bait vectors and screenings were performed according to the manufacturer's instructions. In particular, domains IV and the C-termini of $\text{Ca}_v2.2$ and $\text{Ca}_v2.1$ were cloned into the pBT3-N vector. Since it turned out that $\text{Ca}_v2.1 \text{Ca}^{2+}$ channel constructs did not express in yeast, we used yeast codon-optimized cDNA-fragments of $\text{Ca}_v2.1$. Each screening experiment was performed with about $\sim 1-5 \times 10^6$ transformants. Library plasmids were isolated from *HIS3*- and *ADE2*-positive yeast cells and identified by nucleotide sequencing. To confirm protein-protein-interaction we performed additional assays using PCR-generated full length cDNAs (pPR3N-vector) of the candidate proteins. To analyse the interaction of the individual TSPAN-13-constructs in more detail, we performed a β -galactosidase filter-lift assay according to the manufacturer's instructions.

Pellet- β -galactosidase assay. The pellet- β -galactosidase assay allows for a quantitative estimation of the interaction strength between two proteins expressed in the yeast split-ubiquitin system. This assay was developed by Mückli and Auerbach and is described in⁷. Briefly, yeast colonies were grown to an OD_{546} of 0.8 to 1.0 and then harvested by centrifugation. Yeast cells were broken by repeated freeze-thaw cycles and resuspended in water. The pellet- β -galactosidase assay was performed in 96-well plates by an overlay of the cells with X-Gal-staining solution. Development of blue color was observed using a flat-bed scanner and quantified by the program Multi Gauge V3.0 (Fujifilm, Düsseldorf, Germany).

RT-PCR analysis. Whole brain and hippocampus, neocortex and cerebellum were prepared from cervical dislocated adult male mice. Total RNA was isolated using the RNeasy Midi and Mini kit (Qiagen, Hilden, Germany) according to the manufacturer's protocol. cDNA synthesis was performed by the Transcriptor High Fidelity cDNA synthesis kit (Roche Diagnostics, Mannheim, Germany). Oligonucleotide primers for PCR of TSPAN-13 cDNA were selected from different exons to exclude amplification of genomic DNA. The following primers were used: 5'-CCACGCCACGATGGTGTGCG-3' and 5'-CAGCAGCTGACCCTGCTGCTCCCGA-3'. PCR fragments were verified by sequence analysis.

Plasmids and co-immunoprecipitation (coIP). For cell-imaging and patch-clamp experiments full-length mouse TSPAN-13 and mutants were PCR-generated and cloned into pEGFP-N1 (Clontech, Saint-Germain-en-Laye, France). CoIPs were performed using N-terminal Myc-tagged-TSPAN-13 pcDNA3-vectors (Invitrogen Darmstadt, Germany). CHO cells and CHO cells stably expressing $\text{Ca}_v2.2$ were co-transfected with vectors encoding Myc-TSPAN-13. For each coIP-experiment cells of five 10 cm dishes were rinsed with ice-cold PBS pH 7.4 (containing proteinase-inhibitor complete 1:50 Roche (Roche, Mannheim, Germany)), pooled and thoroughly homogenized. After centrifugation (5 min at $800 \times g$ at 4°C) supernatants were separated and membrane-enriched protein fractions were isolated by an additional centrifugation-step ($16000 \times g$ for 2 h at 4°C). Pelleted membranes were resuspended in CL142-buffer (Logopharm, Freiburg, Germany) and final protein concentration was adjusted to 1.25 $\mu\text{g}/\mu\text{l}$. Solubilisation was carried out at 4°C for 16 h under continuous movement, afterwards insoluble material was removed by centrifugation (110 min at $16000 \times g$ at 4°C). Aliquots of solubilized protein (supernatants) and pellets were resolved in SDS-loading buffer and checked for solubilisation efficiency.

Equal amounts of solubilized proteins ($\sim 400-600 \mu\text{l}$, $c = 1.25 \mu\text{g}/\mu\text{l}$) were added to 50 μl DynaBeads® Protein G (Invitrogen, Darmstadt, Germany) and 10 μg anti-Myc antibody (Cell-signalling, Frankfurt, Germany) or 10 μg mouse-IgG-control (Merck, Darmstadt, Germany). After immunoprecipitation (2.5 h at 4°C), beads were washed and proteins were eluted with SDS-buffer (10 min at 45°C) following manufacturer's instructions.

Western blot analysis. Solubilized proteins and eluates obtained from coIP were separated on 7% and 12% SDS-polyacrylamide gels, respectively. The gels were blotted using a "wet-blot-chamber" (Bio-Rad Laboratories, München, Germany) onto nitrocellulose membranes (Carl-Roth, Karlsruhe, Germany). After blocking and washing, membranes were incubated with the primary antibodies anti-Myc-Tag (Cell-signalling, Frankfurt, Germany) or anti-GFP antibody (Abcam Cambridge, United Kingdom). After washing, the secondary antibodies were applied and proteins were detected using an imaging system (LAS-3000 mini, Fujifilm-Europe,



Düsseldorf, Germany) according to the manufacturer's instructions. Secondary antibodies were obtained from mouse IgG-POX from Biomol (Hamburg, Germany). Streptavidin-HRP (Cell Signaling, Frankfurt, Germany) was used to detect biotinylated anti-GFP-antibody.

Cell lines and cultivation. NG108-15 cells were grown in DMEM containing 10% fetal calf serum (FCS), 100 U/ml penicillin–streptomycin and 1 mM sodium pyruvate (PAA Laboratories, Cölbe, Germany) in an atmosphere of 5% CO₂ and 95% air at 37°C. Differentiation of cells was induced by addition of 1 mM cAMP to growth medium containing 1% FCS for 11 days. Measurement of Ca_v3.1 and Ca_v1.2 currents was performed in HEK 293 cells stably transfected with Ca_v3.1 containing plasmids³² or Ca_v1.2 containing plasmids³³, respectively. Measurement of Ca_v2.1 currents was performed in HEK 293 cells transiently transfected with Ca_v2.1-EGFP-N1 vector and vectors encoding α₂δ- and β₃a-subunits³⁴. Cells were grown in DMEM containing 10% FCS, 100 U/ml penicillin–streptomycin and 0.02 mg/ml G418 (Biochrom, Berlin, Germany). A CHO cell line stably transfected with rat α1-Ca_v2.2-EGFP, α₂δ- and β-subunits was provided by B. Fakler, Institute of Physiology II, University of Freiburg. Cells were grown in MEM ALPHA (Life Technologies, Darmstadt, Germany) including 10% FCS, L-glutamine 200 mM, 0.7 mg/ml G418, 0.25 mg/ml hygromycin B and 0.005 mg/ml blasticidin. Cells were harvested from culture flasks and seeded onto 13 mm round glass coverslips (VWR International, Darmstadt, Germany) coated with 0.01% poly-L-lysine. Cells were transfected with the appropriate expression vectors using LipofectAMINE 2000 (Invitrogen, Darmstadt, Germany). If not stated otherwise, cells were incubated for 24 h following transfection before immunocytochemistry, electrophysiological or biochemical experiments.

Electrophysiology and data analysis. Whole cell Ba²⁺ and Ca²⁺ currents were measured using the HEKA-10 patch clamp amplifier (HEKA Electronic, Lambrecht, Germany). The extracellular solution for measurement of IV currents in NG108-15 cells, Ca_v2.1 currents and gating currents in CHO cells stably expressing Ca_v2.2 contained (in millimolar): BaCl₂, 10; (4-(2-hydroxyethyl)-1-piperazineethanesulfonic acid) HEPES, 10; glucose, 5; tetraethylammonium chloride (TEA-Cl), 125; and pH 7.4 (TEA-OH). For measurement of Ca_v2.2 currents in CHO cells and Ca_v3.1 currents in HEK 293 cells an extracellular solution containing BaCl₂, 2; HEPES, 10; glucose, 5; TEA-Cl, 140; and pH 7.4 (TEA-OH) was used. In part of the experiments BaCl₂ was replaced by 2 millimolar CaCl₂. The extracellular solution for measurements of Ca_v1.2 currents in stably transfected HEK 293 cells contained CaCl₂, 10; HEPES, 10; glucose, 10; TEA-Cl, 130; MgCl₂, 1; CsCl, 5 and pH 7.0 (TEA-OH). The intracellular solution for measurement in all cells contained: CsCl, 110; EGTA, 10; MgCl₂, 3; Na₂-ATP, 3; GTP-Tris, 0.6; HEPES, 10; and pH 7.2 (CsOH).

Patch pipettes were made from borosilicate glass (Sutter Instrument, Novato, USA). When filled with the intracellular solution, input resistance was between 1.8 and 4.0 MΩ. The capacitance of individual cells ranged from 5 to 80 pF, depending on the cell line analysed. Capacity transient and series resistance were compensated up to 70% by built-in procedures of the HEKA-10 amplifier. Linear leak current and remaining capacity transients were subtracted using the P/4 procedure. Data were recorded with HEKA Patchmaster 2.43 and analysed offline using HEKA Fitmaster 2.60 and Origin 8.5 software. The holding potential in all experiments was -80 mV, except for measurement of T-type calcium currents where it was -100 mV. The maximal conductance (G_{max}) of calcium channels was estimated by fitting current-voltage curves by combined Boltzmann-Ohm equation.

Measurement and analysis of gating currents. Gating currents were measured at the reversal potential estimated individually for each cell. At such conditions gating currents are not obscured by inward Ca²⁺ currents and there is no need to use Ca²⁺ channel blockers³⁵. The value of the reversal potential for all cells investigated ranged from +75 to +91 mV. The Q-V relationship for the Ca_v2.2 channel saturates above +10 mV³⁵, therefore we can consider the estimated value of Q to be the maximal value for each cell. Five identical traces were recorded and averaged for each cell. Total on-charge was evaluated by integrating the area below gating current trace at the beginning of each depolarizing pulse.

In order to minimize variations potentially caused by individual transfections, we only compared G_{max}/Q_{max} values from the same day from cells transfected either with a control-EGFP plasmid or with specific TSPAN-13 constructs. Results obtained from these pools were then compared for the TSPAN-13 effect. Control groups from all data sets did not differ significantly (ANOVA with Tukey's post-test).

Data analysis and statistics. Data are presented as mean ± SEM. Statistical significance of differences was determined by two-tail unpaired Student's t test or an ANOVA followed by Tukey's post-test or by a nonparametric Mann-Whitney test as appropriate and considered significant when p < 0.05.

Drugs and reagents. All drugs and chemicals were obtained from Sigma-Aldrich, Taufkirchen, Germany except when stated otherwise.

- Catterall, W. A. Voltage-gated calcium channels. *Cold Spring Harb. Perspect. Biol.* **3**, a003947 (2011).
- Berkfeld, H. *et al.* BKCa-Cav channel complexes mediate rapid and localized Ca²⁺-activated K⁺ signaling. *Science* **314**, 615–620 (2006).
- Muller, C. S. *et al.* Quantitative proteomics of the Ca_v2 channel nano-environments in the mammalian brain. *Proc. Natl. Acad. Sci. U. S. A.* **107**, 14950–14957 (2010).
- Suter, B., Kittanakom, S. & Stagljar, I. Two-hybrid technologies in proteomics research. *Curr. Opin. Biotechnol.* **19**, 316–323 (2008).
- Kaesser, P. S. *et al.* RIM proteins tether Ca²⁺ channels to presynaptic active zones via a direct PDZ-domain interaction. *Cell* **144**, 282–295 (2011).
- Stagljar, I., Korostensky, C., Johnsson, N. & te, H. S. A genetic system based on split-ubiquitin for the analysis of interactions between membrane proteins in vivo. *Proc. Natl. Acad. Sci. U. S. A.* **95**, 5187–5192 (1998).
- Mockli, N. & Auerbach, D. Quantitative beta-galactosidase assay suitable for high-throughput applications in the yeast two-hybrid system. *Biotechniques* **36**, 872–876 (2004).
- Kasai, H. & Neher, E. Dihydropyridine-sensitive and omega-conotoxin-sensitive calcium channels in a mammalian neuroblastoma-glioma cell line. *J. Physiol* **448**, 161–188 (1992).
- Liu, J., Tu, H., Zhang, D. & Li, Y. L. Changes of calcium channel mRNA, protein and current in NG108-15 cells after cell differentiation. *Biochem. Biophys. Res. Commun.* **423**, 55–59 (2012).
- Wyatt, C. N., Page, K. M., Berrow, N. S., Brice, N. L. & Dolphin, A. C. The effect of overexpression of auxiliary Ca²⁺ channel subunits on native Ca²⁺ channel currents in undifferentiated mammalian NG108-15 cells. *J. Physiol* **510** (Pt 2), 347–360 (1998).
- Aglar, H. L. *et al.* G protein-gated inhibitory module of N-type (Ca_v2.2) Ca²⁺ channels. *Neuron* **46**, 891–904 (2005).
- Kovalenko, O. V., Metcalf, D. G., DeGrado, W. F. & Hemler, M. E. Structural organization and interactions of transmembrane domains in tetraspanin proteins. *BMC Struct. Biol.* **5**, 11 (2005).
- Min, G., Wang, H., Sun, T. T. & Kong, X. P. Structural basis for tetraspanin functions as revealed by the cryo-EM structure of uroplakin complexes at 6-Å resolution. *J. Cell Biol.* **173**, 975–983 (2006).
- Boucheix, C. & Rubinstein, E. Tetraspanins. *Cell Mol. Life Sci.* **58**, 1189–1205 (2001).
- Berditchevski, F. Complexes of tetraspanins with integrins: more than meets the eye. *J. Cell Sci.* **114**, 4143–4151 (2001).
- Hemler, M. E. Tetraspanin functions and associated microdomains. *Nat. Rev. Mol. Cell Biol.* **6**, 801–811 (2005).
- Hemler, M. E. Targeting of tetraspanin proteins—potential benefits and strategies. *Nat. Rev. Drug Discov.* **7**, 747–758 (2008).
- Barreiro, O. *et al.* Endothelial tetraspanin microdomains regulate leukocyte firm adhesion during extravasation. *Blood* **105**, 2852–2861 (2005).
- Shoham, T., Rajapaksa, R., Kuo, C. C., Haimovich, J. & Levy, S. Building of the tetraspanin web: distinct structural domains of CD81 function in different cellular compartments. *Mol. Cell Biol.* **26**, 1373–1385 (2006).
- Zevian, S., Winterwood, N. E. & Stipp, C. S. Structure-function analysis of tetraspanin CD151 reveals distinct requirements for tumor cell behaviors mediated by alpha3beta1 versus alpha6beta4 integrin. *J. Biol. Chem.* **286**, 7496–7506 (2011).
- Charrin, S. *et al.* Lateral organization of membrane proteins: tetraspanins spin their web. *Biochem. J.* **420**, 133–154 (2009).
- Yanez-Mo, M., Sanchez-Madrid, F. & Cabanas, C. Membrane proteases and tetraspanins. *Biochem. Soc. Trans.* **39**, 541–546 (2011).
- Huang, H., Sossey-Alaoui, K., Beachy, S. H. & Geradts, J. The tetraspanin superfamily member NET-6 is a new tumor suppressor gene. *J. Cancer Res. Clin. Oncol.* **133**, 761–769 (2007).
- Kurejova, M., Lacinova, L., Pavlovicova, M., Eschbach, M. & Klugbauer, N. The effect of the outermost basic residues in the S4 segments of the Ca_v3.1 T-type calcium channel on channel gating. *Pflugers Arch.* **455**, 527–539 (2007).
- Talavera, K., Janssens, A., Klugbauer, N., Droogmans, G. & Nilius, B. Extracellular Ca²⁺ modulates the effects of protons on gating and conduction properties of the T-type Ca²⁺ channel alpha1G (Ca_v3.1). *J. Gen. Physiol.* **121**, 511–528 (2003).
- Liang, H. *et al.* Unified mechanisms of Ca²⁺ regulation across the Ca²⁺ channel family. *Neuron* **39**, 951–960 (2003).
- Kim, E. Y. *et al.* Structures of Ca_v2 Ca²⁺/CaM-IQ domain complexes reveal binding modes that underlie calcium-dependent inactivation and facilitation. *Structure*. **16**, 1455–1467 (2008).
- McNaughton, N. C. & Randall, A. D. Electrophysiological properties of the human N-type Ca²⁺ channel: I. Channel gating in Ca²⁺, Ba²⁺ and Sr²⁺ containing solutions. *Neuropharmacology* **36**, 895–915 (1997).
- Jones, L. P., DeMaria, C. D. & Yue, D. T. N-type calcium channel inactivation probed by gating-current analysis. *Biophys. J.* **76**, 2530–2552 (1999).
- Grassi, F. & Lux, H. D. Voltage-dependent GABA-induced modulation of calcium currents in chick sensory neurons. *Neurosci. Lett.* **105**, 113–119 (1989).
- Zamponi, G. W. & Snutch, T. P. Decay of prepulse facilitation of N type calcium channels during G protein inhibition is consistent with binding of a single Gbeta subunit. *Proc. Natl. Acad. Sci. U. S. A.* **95**, 4035–4039 (1998).
- Lacinova, L., Kurejova, M., Klugbauer, N. & Hofmann, F. Gating of the expressed T-type Ca_v3.1 calcium channels is modulated by Ca²⁺. *Acta Physiol (Oxf)* **186**, 249–260 (2006).
- Zong, X. *et al.* On the regulation of the expressed L-type calcium channel by cAMP-dependent phosphorylation. *Pflugers Arch.* **430**, 340–347 (1995).



34. Klugbauer, N. *et al.* A family of gamma-like calcium channel subunits. *FEBS Lett.* **470**, 189–197 (2000).
35. Yarotsky, V. & Elmslie, K. S. Open-state occupancy prevents gating charge relaxation of N-type (CaV2.2) calcium channels. *Biophys. J.* **97**, 2446–2455 (2009).

Acknowledgments

We thank U. Christoph for technical assistance and C. Schwan for preparing microscopy figures. We also thank Winfried Römer for providing us with the pAkt-PH-mCherry membrane marker plasmid. The article processing charge was funded by the German Research Foundation (DFG) and the Albert Ludwigs University Freiburg in the funding program Open Access Publishing.

Author contributions:

R.M. and T.W. acquired, analysed and interpreted data; wrote the paper. L.Li and A.B. acquired, analysed and interpreted data. B.L. provided critical experimental expertise and technology. J.C. provided critical reagent and helped acquire data. L.La provided critical experimental expertise and technology; designed electrophysiological experiments and interpreted data; wrote the paper. N.K. conceived and designed experiments and interpreted data; wrote the paper.

Additional information

Supplementary information accompanies this paper at <http://www.nature.com/scientificreports>

Competing financial interests: The authors declare no competing financial interests.

License: This work is licensed under a Creative Commons Attribution-NonCommercial-NoDerivs 3.0 Unported License. To view a copy of this license, visit <http://creativecommons.org/licenses/by-nc-nd/3.0/>

How to cite this article: Mallmann, R. *et al.* Tetraspanin-13 modulates voltage-gated Ca_v2.2 Ca²⁺ channels. *Sci. Rep.* **3**, 1777; DOI:10.1038/srep01777 (2013).